



## Structural and electrical characteristics of gallium modified PZT ceramics

Pulkit Sharma<sup>1</sup>, Sugato Hajra<sup>1</sup>, Sushrisangita Sahoo<sup>2</sup>, Pravat Kumar Rout<sup>1,\*</sup>,  
Ram Naresh Prasad Choudhary<sup>2</sup>

<sup>1</sup>Department of Electrical and Electronics Engineering, Siksha O Anusandhan University, Bhubaneswar - 751030, India

<sup>2</sup>Multifunctional and Advanced Materials Research Lab, Department of Physics, Siksha O Anusandhan University, Bhubaneswar- 751030, India

Received 3 April 2017; Received in revised form 21 May 2017; Received in revised form 10 June 2017;

Accepted 20 June 2017

### Abstract

In the present paper, the gallium modified lead zirconate titanate ceramics with Zr/Ti = 48/52 (near the morphotropic phase boundary, MPB), having a chemical formula  $Pb_{0.98}Ga_{0.02}(Zr_{0.48}Ti_{0.52})_{0.995}O_3$ , was synthesized by a mixed-oxide reaction method and sintered. Analysis of phase formation confirmed the co-existence of two phases (tetragonal and monoclinic symmetry) in the system. Microstructural study by scanning electron microscope showed a non-uniform distribution of large grains over the sample surface and presence of a small amount of micro-size pores. Modulus and impedance studies were carried out at various frequencies (1 kHz–1 MHz) and temperatures (300–350 °C) and showed the contributions of grains in capacitive and resistive properties of the material. The resistance and capacitance of the complex impedance plots are contributed by grains as observed from the Nyquist plots. The experimental data obtained from the Nyquist plot were implemented in an equivalent electrical circuit (RQC). The value of grain resistance and capacitance were obtained using fitting steps with precision at all temperatures. It is assumed that increase of dielectric constant at higher temperatures is due to the substitution of  $Ga^+$  ions at the Pb-site.

**Keywords:**  $Pb(Zr,Ti)O_3$ , solid-state synthesis, structural characterization, electrical and dielectric properties

### I. Introduction

Lead based ferroelectrics belonging to perovskite structural family are widely used for some industrial applications, such as, bypass capacitor, micro electric motors, FeRAM/DRAM capacitors, linear gate arrays, and other ferroelectric related devices [1–5]. They have drawn lot of attention of material scientists due to the existence of their excellent ferroelectric, dielectric and piezoelectric properties [6,7]. One of the lead based compounds, lead zirconate titanate  $Pb(Zr,Ti)O_3$  (PZT) belongs to the perovskite structural family of a general formula  $ABO_3$  in which  $Pb^{2+}$  and  $Zr^{4+}/Ti^{4+}$  ions occupy the A- and B-sites, respectively, by maintaining proper electrical neutrality and structural stability. PZT

is formed by combination of ferroelectric  $PbTiO_3$  ( $T_c = 490\text{ }^\circ\text{C}$ ) and antiferroelectric  $PbZrO_3$  ( $T_c = 230\text{ }^\circ\text{C}$ ) with various ratios of Zr/Ti [8]. The presence of defects, dipoles and phase boundaries contributes to the extrinsic characteristics of the materials [9]. The physical properties of the material are strongly affected by deviations of many factors, such as, charge neutrality, solubility and ionic radius. The most important factor among them is Zr/Ti ratio which strongly affects the physical properties and the existence of different structural phases (tetragonal, rhombohedral and orthorhombic) in PZT at room temperature. Though structural and physical properties of PZT have been tailored by various substitutions at the A/B-sites, the gallium (Ga) substitution at the Pb-sites leads to a considerable A-site disordering which fulfils the vacancies created by  $Pb^{+2}$ . The long range ordering of ferroelectrics gets unsettled due to the occurrence of two types of defects. The detailed literature survey has

\*Corresponding author: tel: +91 9337261952,  
e-mail: [pkrou\\_t\\_india@yahoo.com](mailto:pkrou_t_india@yahoo.com)

shown that the work on gallium-substituted PZT was not previously conducted. This has attracted us to carry out the systematic studies on Ga-substituted PZT in MPB region (Zr/Ti = 48/52), which has not been reported earlier except some work on rare earth ions modified PZT [10]. Therefore, an initiative attempt has been made to study the effect of small amounts (2 at.%) of Ga substitution on structural, microstructural, dielectric and electric properties of  $\text{Pb}_{0.98}\text{Ga}_{0.02}(\text{Zr}_{0.48}\text{Ti}_{0.52})_{0.995}\text{O}_3$  ceramics.

## II. Experimental

### 2.1. Sample preparation

Lead monoxide (Loba Chemie Pvt. Ltd., India, 99%-purity), titanium dioxide (Loba Chemie Pvt. Ltd., India, 99.5%-purity), gallium oxide (OTTO-Chemika-Biochemica-Reagents, 99.999%-purity) and zirconium oxide (Himedia Chemie Pvt. Ltd., India, 99%-purity) were used as raw materials for the synthesis of PGaZT-2 sample.

All the oxides were weighed (according to the stoichiometry), and thoroughly mixed in an agate mortar. The homogeneous mixture was obtained by dry grinding, followed by wet grinding in methanol until the methanol evaporated from the agate mortar. The mixed powder was put into a high-temperature furnace using an alumina crucible with alumina cover and calcined at 1000 °C for 12 h. To maintain desired stoichiometry, Pb loss was compensated by initially adding 2 wt.% excess of PbO, and heating the material in covered crucible. The disc shaped pellets were fabricated from the calcined powder uni-axially compacted at pressure of  $4 \times 10^6 \text{ N/m}^2$ . The pellets were sized to a diameter of 12 mm and thickness of 0.1–0.2 cm. Polyvinyl alcohol (PVA) was used as a binder to facilitate the compactness of the powder. The sintering was carried out through a conventional, but a cost effective sintering process at 970 °C for 4 h. The prepared sample ( $\text{Pb}_{0.98}\text{Ga}_{0.02}(\text{Zr}_{0.48}\text{Ti}_{0.52})_{0.995}\text{O}_3$ ) hereafter is referred as PGaZT-2.

The surface of the sintered discs was polished and painted with high-conductive silver paint. The conductive silver paste was applied to both parallel surfaces of pellets for carrying out electrical (dielectric, impedance, conductivity and modulus characteristics) measurements. The silver coated samples were dried in a high temperature oven at 150 °C for 2 h before electrical measurements.

### 2.2. Characterization

X-ray diffraction data of the sample were collected with Bruker D8 Advance diffractometer with increment of  $0.052^\circ$  and measuring time of 0.75 s using  $\text{CuK}\alpha$  radiation in Bragg's angle range  $20^\circ \leq 2\theta \leq 80^\circ$ . A gold-coated sample was used to investigate the texture and microstructure of the material surface at different magnifications, using field emission scanning electron

microscope (FESEM, ZEISS SUPRA 40) operated at 5 kV. The electrode was connected to the samples using a silver paint with zero contact resistance for dielectric and loss analysis. The measurements of electric and dielectric properties were performed using a computer-controlled phase sensitive meter (PSM LCR 4NL: 1735, UK) at variable frequency (1 kHz to 1 MHz) and in temperature range 300–350 °C. A thermocouple coupled with sample holder was placed in a laboratory-fabricated furnace.

## III. Results and discussion

### 3.1. Structural and microstructural analysis

Figure 1 shows a room temperature XRD pattern of the powder sample which indicates the formation of two phases (major tetragonal symmetry and minor monoclinic symmetry). The matched PZT peaks correspond to the tetragonal phase and extra prominent peaks represent minor monoclinic phases. The PZT peaks were compared with reference ones by using “Match Powder Diffraction” software. The reflection peaks of the pattern were indexed by using available commercial software called “POWD- MULT” [11]. As expected, the high intensity peak of the sample is observed at around  $32^\circ$ . The co-existence of two phases observed in the XRD pattern might be due to many reasons like metastable coexistence, solubility gap, fluctuation in the composition (rate of diffusion of Ti is much higher than the rate of diffusion of Zr) [12–14].

Figure 2 shows the micrograph image of the PGaZT-2 pellet recorded with field emission scanning electron microscope at room temperature. Some pores are found in the sample due to the improper treatment of the PVA binder. The surface texture has non-uniform distribution with polycrystalline grains of different shape and size. Thus, microstructure also highlights formation of two-phase system. It also clearly confirms a high-density grain growth and a small degree of porosity in the sample.

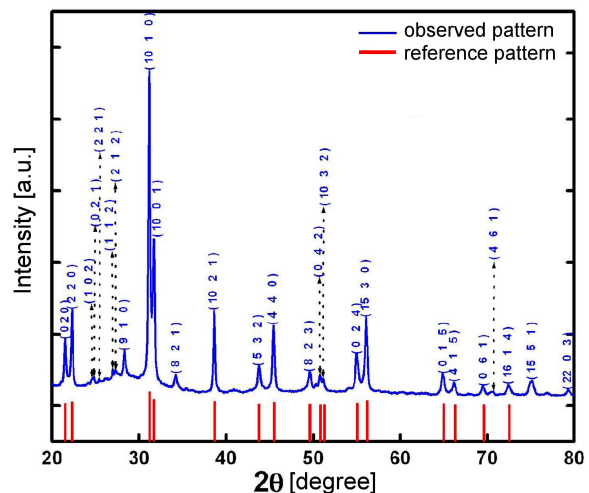


Figure 1. XRD pattern of PGaZT-2 sample

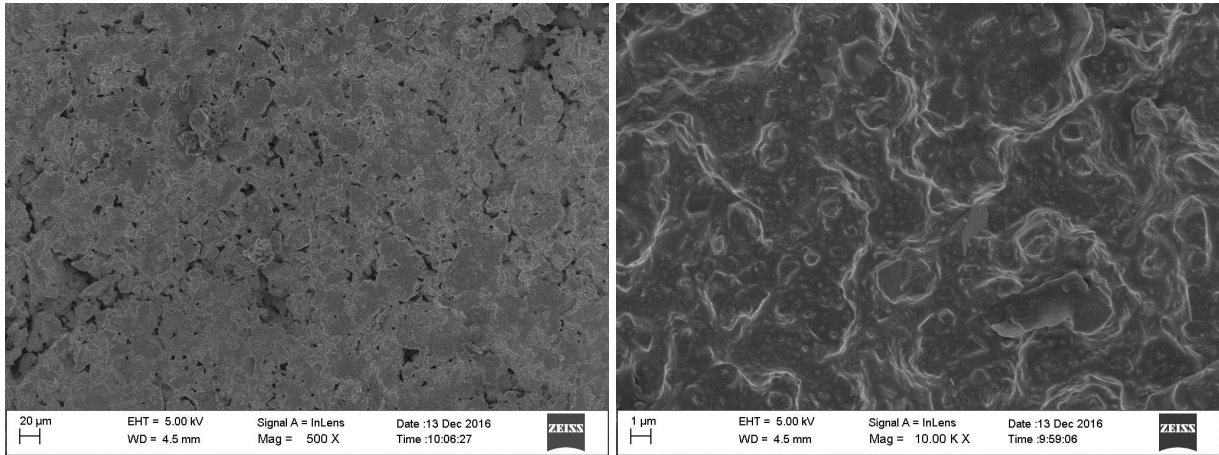


Figure 2. FESEM micrographs of sintered PGaZT-2 sample

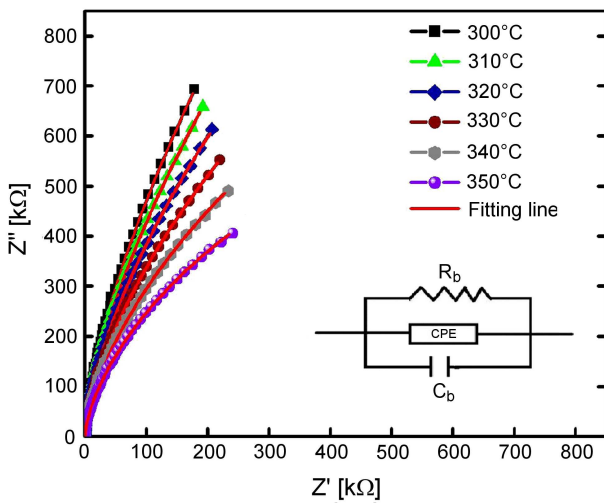


Figure 3. Variation of  $Z'$  vs  $Z''$  at various temperatures (Nyquist plot)

### 3.2. Impedance spectroscopy

Complex impedance spectroscopy (CIS), a non-destructive method, is used to study the electrical behaviour of the material at various temperatures and frequencies. The real ( $Z'$ ) and imaginary ( $Z''$ ) components of complex impedance can easily be separated by this method, and the material properties are truly highlighted. By using the CIS method, symmetric and asymmetric (depressed) arcs might generally be observed in the  $Z''$ - $Z'$  plots. In the case of asymmetric arcs the ideal capacitor (Debye type) cannot be used for fitting the data and modified formula should be applied [16].

The complex impedance components can be written as [16]:

$$Z^* = Z' + j \cdot Z'' \quad (1)$$

$$Z' = \frac{R}{(1 + \omega \cdot \tau)^2} \quad (2)$$

$$Z'' = \frac{\omega \cdot R \cdot \tau}{(1 + \omega \cdot \tau)^2} \quad (3)$$

In CIS technique, we apply an alternating voltage

signal to the sample, and obtain corresponding phase shifted current response. The real ( $Z'$ ) and imaginary ( $Z''$ ) components of the complex (\*) electrical parameters, such as  $Z$  (impedance), modulus ( $M$ ), and dielectric constant ( $\epsilon$ ), can be separated by the CIS technique. Impedance data containing capacitance, resistance and angular frequency can be analysed by using Nyquist plots leading to corresponding semicircles. An equivalent circuit traced with impedance and modulus data collected in different experimental conditions (temperature, frequency) is used to understand a physical process and mechanism in the material. The presence of frequency peaks on semicircles can be explained on the basis of following equation  $2\pi \cdot f_{max} \cdot \tau = 1$ , where  $\tau$  is the mean relaxation time. The non-Debye condition can also be clearly detected and is characterized with presence of imperfect semicircular arcs [17,18].

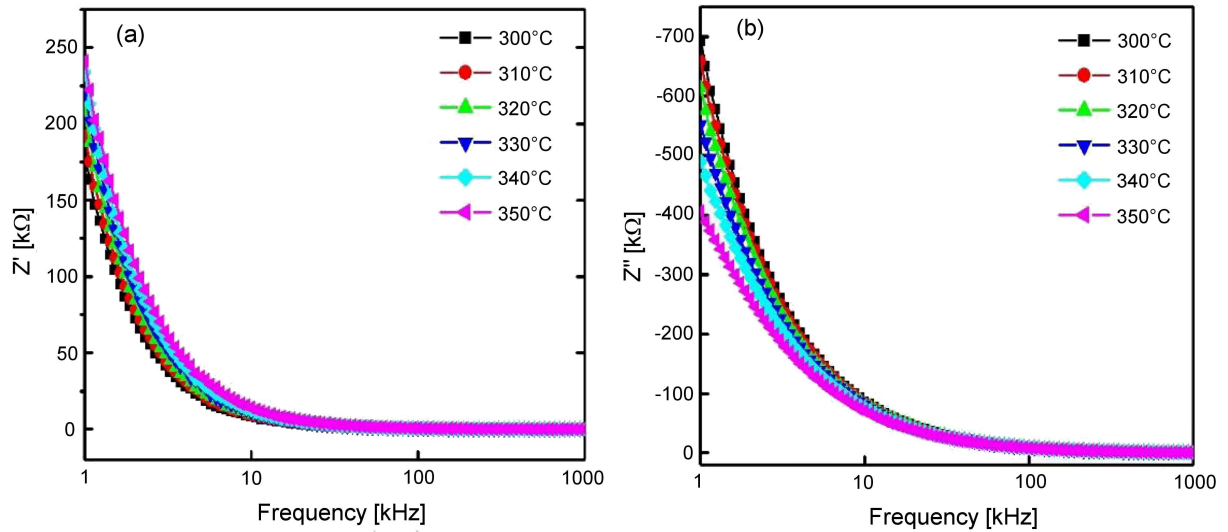
Figure 3 shows the complex impedance spectra (Nyquist plot), at various temperatures (300–350 °C), of the sintered PGaZT-2 sample. It seems that the spectra show a depressed arc whose evolution pattern changes upon a rise in the temperature. By using ZSIMP WIN Version 2 software, the observed data are compared with a theoretically fitted data (solid line) and the fitted parameters of the bulk resistance ( $R_b$ ), bulk capacitance ( $C_b$ ) along with bulk DC conductivity ( $\sigma_{DC}$ ) are shown in Table 1.

Figure 4a determines the variation of the real part of impedance as a function of frequency at different temperatures (300–350 °C) for the sintered PGaZT-2 sample. It can be seen that  $Z'$  decreases with a rise in temperature, which clearly indicates the negative temperature coefficient of resistance (NTCR) in the sample. The variation of the imaginary part of the impedance with frequency at various temperatures (300–350 °C), presented in Fig. 4b, shows that there is continuous decrease of  $Z''$  with frequency without any distinguishable peak. In general, the presence of a peak suggests that the relaxation process is associated with the material. The decrease in  $Z''$  with rise in temperature is caused due to the absence of mobile electrons at the investigated temperatures [19].

**Table 1.** Values of grain capacitance ( $C_g$ ), grain resistance ( $R_g$ ) and bulk conductivity ( $\sigma_{DC}$ ) for sintered PGaZT-2 sample at various temperatures

Temperature [ $^{\circ}\text{C}$ ]	$R_g$ [ $\Omega$ ]	$C_g$ [F]	$\sigma_{DC}$ [ $\Omega^{-1}\text{m}^{-1}$ ] <sup>a</sup>
300	$1.381 \times 10^8$	$1.667 \times 10^{-10}$	$8.200 \times 10^{-8}$
310	$7.430 \times 10^7$	$1.683 \times 10^{-10}$	$1.444 \times 10^{-7}$
320	$1.279 \times 10^7$	$1.695 \times 10^{-10}$	$8.601 \times 10^{-7}$
330	$5.851 \times 10^6$	$1.707 \times 10^{-10}$	$1.835 \times 10^{-6}$
340	$4.329 \times 10^6$	$1.730 \times 10^{-10}$	$2.481 \times 10^{-6}$
350	$2.490 \times 10^6$	$1.756 \times 10^{-10}$	$4.314 \times 10^{-6}$

$$^a \sigma_{DC} = t/R_g \cdot A$$



**Figure 4.** Variation of  $Z'$  (a) and  $Z''$  (b) with frequency at different temperatures for sintered PGaZT-2 sample

### 3.3. Dielectric properties

Figure 5 exhibits the variation of relative dielectric constant  $\epsilon_r$  with temperature at various frequencies (1, 10 and 100 kHz) for the sintered PGaZT-2 sample. It clearly shows that there is almost constant  $\epsilon_r$  value up to  $\sim 200^{\circ}\text{C}$ , and an increase in the dielectric constant with further rise in temperature to its maximum value. Behera *et al.* [20] observed the ferroelectric to paraelectric phase transition for PZT ceramics at around  $432^{\circ}\text{C}$  at frequency of 100 kHz. The trend of disappearance of  $T_c$  at MPB or its movement towards higher temperature is considered, as the elementary dipoles merge with each other giving rise to an internal field which aligns dipoles. Moreover, the non-occurrence of ferroelectric-paraelectric phase transition is accompanied by the polar/non-polar symmetry change with crystal polarization loss. Though this observation is controversial, it can be restructured by the reconstructive transitional characteristics and by the structural hindrances in the low-temperature phase [21].

Figure 6 shows that the dielectric constant of the doped PZT sample decreases with a rise in frequency at selected temperatures. The polarizations at lower frequency due to interfacial, ionic, dipolar and electronic contributions, and cause the observed high values of  $\epsilon_r$  [22]. The dielectric constant decreases with

decrease in frequency, as some of the polarizations become ineffective. Thus, the interfacial polarizations play an important role at low frequencies, but it was ineffective at higher frequencies.

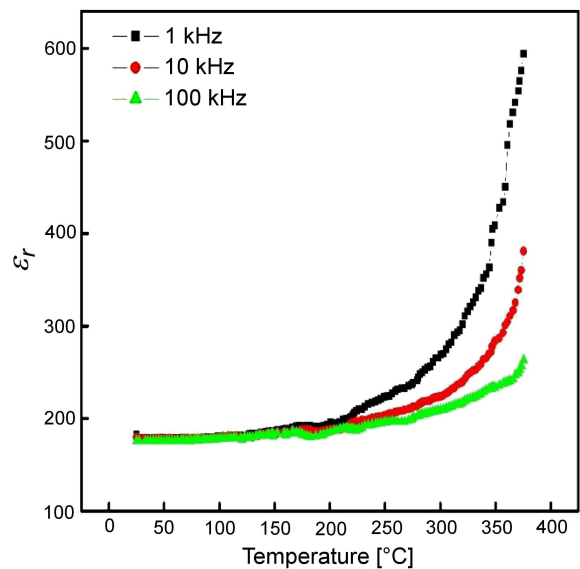


**Figure 5.** Variation of dielectric constant  $\epsilon_r$  with temperature at frequencies 1, 10 and 100 kHz

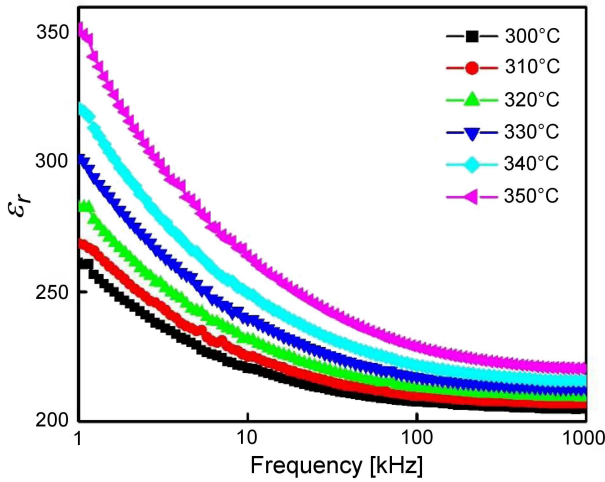


Figure 6. Variation of dielectric constant  $\epsilon_r$  with frequency at different temperatures (300–350 °C)

### 3.4. AC conductivity analysis

Variation of AC conductivity (determined by following relation  $\sigma_{AC} = \omega \cdot \epsilon_0 \cdot \epsilon_r \cdot \tan \delta$ ) with frequency at some preferred temperatures is presented in Fig. 7. AC conductivity progressively rises with temperature increase. The rise of AC conductivity can be explained with a thermally-activated electrical conduction of charge carriers. It is well known that the oxygen vacancies created during material processing decrease activation energy in ceramic technology. In perovskite ferroelectrics, oxygen vacancies are usually considered as primary mobile charge carriers [23,24]. The Jonscher’s equation:  $\sigma_{AC} = A \cdot \omega^n$  was used to fit the frequency response of AC conductivity data. The parameters ( $A$ ,  $n$ ) fitted at various temperatures of the sintered PGaZT-2 sample are given in Table 2.

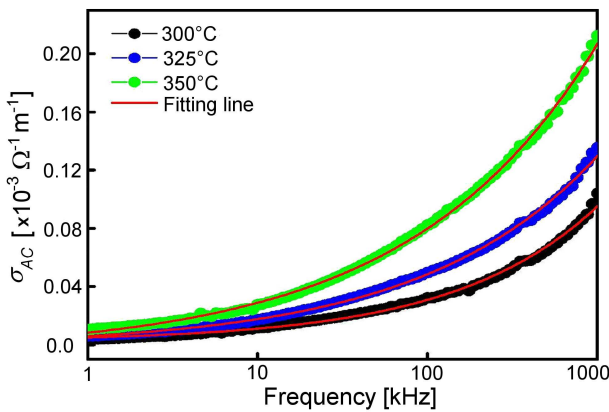


Figure 7. Deviation of AC conductivity with frequency at different temperatures for sintered PGaZT-2 sample

Table 2. Jonscher’s universal law, AC conductivity fitting parameters of PGaZT-2

Temperature [°C]	$n$	$A$
300	0.51177	$7.892 \times 10^{-8}$
325	0.42052	$3.926 \times 10^{-7}$
350	0.39537	$9.014 \times 10^{-7}$

### 3.5. Modulus characteristics

The materials which inherit the same resistance, but varying capacitances can be determined by electrical modulus spectroscopy plots. The other reason of this formalism is to verify the effect of electrode, which should be suppressed in our material. Due to these reasons, the complex electric modulus has been chosen. Study on complex modulus  $M^*$  formalism also gives us the idea about the relaxation process associated with the material. The variations of real ( $M'$ ) and imaginary ( $M''$ ) parts of the electric modulus as a function of frequency at various temperatures are shown in Fig. 8. As shown in Fig. 8a, at higher frequencies,  $M'$  achieves a steady value. It confirms the presence of possible ionic polarization as at lower frequencies  $M'$  reaches 0. The variation of  $M'$  from low-frequency limit to high-frequency limit increases. As temperature increases, the dispersion shifts towards higher frequencies [25].

It was also found that  $M''$  decreases with frequency and attains a constant value at higher frequency at all investigated temperatures (Fig. 8b). The position of  $M''$  curve moves towards the higher frequency and the nature of dielectric relaxation suggests that the hop-

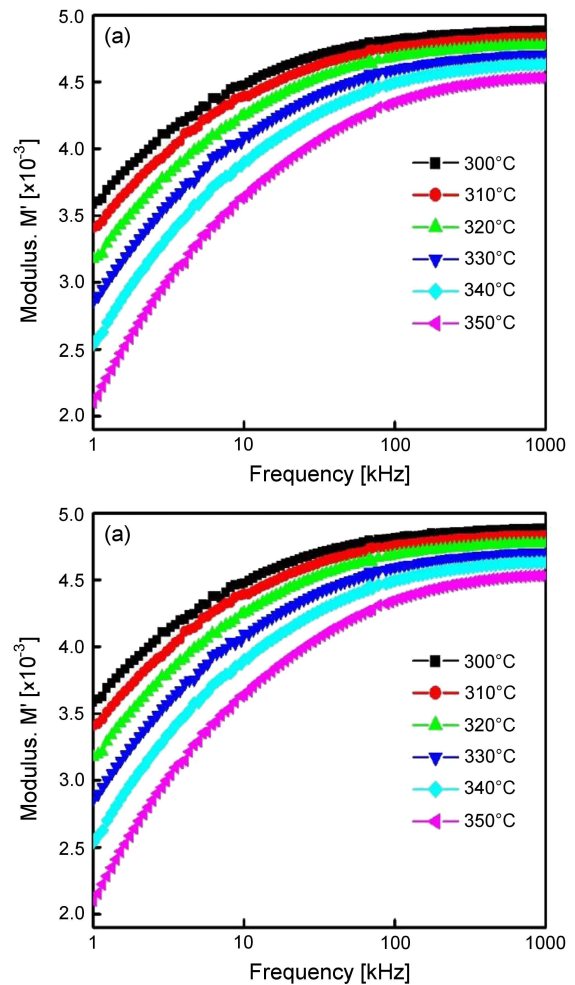


Figure 8. Variation of  $M'$  (a) and  $M''$  (b) with frequency at different temperatures (300–350 °C) for sintered PGaZT-2 sample

ping mechanism of charge carriers seizes intrinsically at higher temperature. The spread of relaxation with different time constants indicates the asymmetric nature, highlighting the existence of the non-Debye type relaxation process in the material [26].

#### IV. Conclusions

Gallium modified lead zirconate titanate ( $\text{Pb}_{0.98}\text{Ga}_{0.02}(\text{Zr}_{0.48}\text{Ti}_{0.52})_{0.995}\text{O}_3$ ) ceramics, with Zr/Ti near the morphotropic phase boundary, was synthesized by the mixed oxide reaction route and conventionally sintered. The study of crystal structure, surface morphology, dielectric and electrical characteristics of the material were carried out thoroughly. The structural analysis confirmed the co-existence of two phases (tetragonal and monoclinic symmetry), non-uniform distribution of large grains over the sample surface and presence of a small amount of micro-size pores. The complex impedance spectroscopy showed the semiconducting behaviour of the sintered Ga-modified PZT ceramics. The analysis of impedance and modulus characteristics indicated on non-Debye relaxation and significant contributions of grains on electrical properties. The frequency and temperature response of conductivity was also analysed by Jonscher's power law and Arrhenius relation, respectively.

**Acknowledgements:** The authors express their gratitude to Mr. Uttam Kumar Chandra and Mr. Manas Kumar Sahoo of School of Minerals, Metallurgical & Materials Engineering, Indian Institute of Technology Bhubaneswar for their kind help in the experimental work.

#### References

1. G. Akcay, S.P. Alpay, G.A. Rossetti, J.F. Scott, "Influence of mechanical boundary conditions on the electrocaloric properties of ferroelectric thin films", *J. Appl. Phys.*, **103** (2008) 024104.
2. J.F. Scott, "Applications of modern ferroelectrics", *Science*, **315** (2007) 954–959.
3. J.F. Scott, C.A.P. Dearaujo, "Ferroelectric memories", *Science*, **246** (1989) 1400–1405.
4. G.H. Haertling, "Ferroelectric ceramics: History and technology", *J. Am. Ceram. Soc.*, **86** (1999) 797–818.
5. M.E. Lines, A.M. Glass, *Principles and Applications of Ferroelectrics and Related Materials*, New York, Oxford University Press, 1977.
6. C. Duran, S.T. McKinstry, G.L. Messing, "Processing and electrical properties of  $0.5\text{Pb}(\text{Yb}_{1/2}\text{Nb}_{1/2})\text{O}_3 - 0.5\text{PbTiO}_3$  ceramics", *J. Electroceram.*, **10** (2003) 47–55.
7. P. Lua, M. Zhu, W. Zou, Z. Li, C. Wang, "Low-temperature sintering of PNW-PMN-PZT piezoelectric ceramics", *J. Mater. Res.*, **22** (2007) 2410–2415.
8. T. Maiti, R. Guo, A.S. Bhalla, "Enhanced electric field tunable dielectric properties of  $\text{BaZr}_x\text{Ti}_{1-x}\text{O}_3$  relaxor ferroelectrics", *Appl. Phys. Lett.*, **90** (2007) 182901.
9. G. Arlt, H. Dederichs, R. Herbiet, "90°-domain wall relaxation in tetragonally distorted ferroelectric ceramics", *Ferroelectrics*, **74** (1987) 37–53.
10. X. Dai, A. DiGiovanni, D. Viehland, "Dielectric properties of tetragonal lanthanum modified lead zirconate titanate ceramics", *J. Appl. Phys.*, **74** (1993) 3399–3405.
11. E. Wu, *POWDMULT: An interactive powder diffraction data interpretation and indexing program version 2.1*, School of Physical sciences, Flinders University of South Australia, 1989.
12. A.P. Wilkinson, J. Xu, S. Pattanaik, S.J.L. Billinge, "Neutron scattering studies of compositional heterogeneity in sol-gel processed lead zirconate titanates", *Chem. Mater.*, **10** (1998) 3611–3619.
13. S.A. Mabud, "The morphotropic phase boundary in PZT solid solutions", *J. Appl. Crystallogr.*, **13** (1980) 211–216.
14. Y. Wang, "Diffraction theory of nanotwin superlattices with low symmetry phase", *Phys. Rev. B*, **74** (2006) 104109.
15. N. Sahu, S. Panigrahi, "Rietveld analysis, dielectric and impedance behaviour of  $\text{Mn}^{3+}/\text{Fe}^{3+}$  ion modified  $\text{Pb}(\text{Zr}_{0.65}\text{Ti}_{0.35})\text{O}_3$  perovskite", *Bull. Mater. Sci.*, **36** (2013) 699–708.
16. S.C. Panigrahi, P.R. Das, B.N. Parida, H.B.K. Sharma, R.N.P. Choudhary, "Effect of Gd-substitution on dielectric and transport properties of lead zirconate titanate ceramics", *J. Mater. Sci.: Mater. Electron.*, **24** (2013) 3275–3283.
17. S. Sahoo, P.K. Mahapatra, R.N.P. Choudhary, M.L. Nandagoswami, A. Kumar, "Structural, electrical and magnetic characteristics of improper multiferroic:  $\text{GdFeO}_3$ ", *Mater. Res. Express*, **3** (2016) 065017.
18. J. Xia, Q. Zhao, B. Gao, A. Chang, B. Zhang, P. Zhao, R. Maa, "Sintering temperature and impedance analysis of  $\text{Mn}_{0.9}\text{Co}_{1.2}\text{Ni}_{0.27}\text{Mg}_{0.15}\text{Al}_{0.03}\text{Fe}_{0.45}\text{O}_4$  NTC ceramic prepared by W/O microemulsion method", *J. Alloys Compd.*, **617** (2014) 228–234.
19. S. Maity, D. Bhattacharya, S.K. Ray, "Structural and impedance spectroscopy of pseudo-co-ablated  $(\text{SrBi}_2\text{Ta}_2\text{O}_9)_{(1-x)}-(\text{La}_{0.67}\text{Sr}_{0.33}\text{MnO}_3)_x$  composites", *J. Phys. D: Appl. Phys.*, **44** (2011) 095403.
20. C. Behera, P.R. Das, R.N.P. Choudhary, "Structural and electrical properties of mechanothermally synthesized  $\text{NiFe}_2\text{O}_4$  nanoceramics", *J. Electron. Mater.*, **43** (2014) 3539–3549.
21. M. Szafranski, M. Jarek, "Origin of spontaneous polarization and reconstructive phase transition in guanidinium iodide", *Cryst. Eng. Comm.*, **15** (2013) 4617.
22. S. Sahoo, P.K. Mahapatra, R.N.P. Choudhary, "Effect of sintering temperature on dielectric, electrical and magneto-electric characteristics of chemico-thermally synthesized  $(\text{Ba}_{0.9}\text{Gd}_{0.1})(\text{Ti}_{0.9}\text{Fe}_{0.1})\text{O}_3$ ", *Ceram. Int.*, **42** (2016) 15955–15967.
23. B. Garbarz-Glos, W. Bąk, M. Antonova, M. Pawlik, "Structural, microstructural and impedance spectroscopy study of functional ferroelectric ceramic materials based on barium titanate", *Mater. Sci. Eng.*, **49** (2013) 012031.
24. T. Acharya, R.N.P. Choudhary, "Development of ilmenite-type electronic material  $\text{CdTiO}_3$  for devices", *IEEE Trans. Dielec. Electric. Insulation*, **22** (2015) 3521–3528.
25. B.C. Sutar, P.R. Das, R.N.P. Choudhary, "Synthesis and electrical properties of  $\text{Sr}(\text{Bi}_{0.5}\text{V}_{0.5})\text{O}_3$  electroceramic", *Adv. Mater. Lett.*, **5** (2014) 131–137.
26. J. Ross McDonald, "Note on the parameterization of the constant-phase admittance element", *Solid State Ionics*, **13** (1984) 147–149.